J Nanostruct 16(3): 3280-3295, Summer 2026

RESEARCH PAPER

Synthesis and Characterization of a Schiff Base Ligand Derived from Diacetyl Monoxime, and the Study of Its Ag(I) Nanocomplex and Evaluation of Their Biological Activity

Eman Jubiar [1], Ghusoon Faidhi [2], and Shaimaa Adnan [2]*

[1] *Ministry of Education General Directorate of Al-Qadisiyah Education, Diwaniyah, Iraq*

[2] *Department of Chemistry, College of Education, University of Al-Qadisiyah, Diwaniyah, Iraq*

ARTICLE INFO

Article History:
Received 09 March 2026
Accepted 15 May 2026
Published 01 July 2026

Keywords:
Ag(I) Nanocomplex
Antioxidant activity
Cytotoxicity (A549)
Diacetyl Monoxime

ABSTRACT

The work in this paper describes the preparation and characterization of a new Silver (I) complex that is bonded with a Schiff Base Ligand synthesized from Diacetylmonoxime. A full range of analytical techniques have been used to determine fully the structure and the physical properties of both the ligand and the resultant complex. These include FT-IR, UV-Vis, ^{1}H and ^{13}C NMR Spectroscopy, Mass Spectrometry and Elemental Analysis (C, H, N), Crystallographic (X-Ray Diffraction) and Morphological (Field Emission Scanning Electron Microscopy) studies of the solid state complex, Thermogravimetric Analysis (TGA) of the solid state complex's thermal decomposition, and Atomic Absorption, Magnetic Susceptibility, and Molar Conductivity measurements for the determination of the complex's key physical/chemical parameters. Biological activity, selectivity, and potential therapeutic efficacy of the ligand and the complex was examined in cytotoxicity studies with lung cancer cells (A549) and normal cells (WRL-68). Additionally, we conducted an antioxidant study with the DPPH free radical scavenger assay and compared the results to that of regular ascorbic acid.

How to cite this article
Jubiar E., Faidhi G., Adnan S. Synthesis and Characterization of a Schiff Base Ligand Derived from Diacetyl Monoxime, and the Study of Its Ag(I) Nanocomplex and Evaluation of Their Biological Activity. J Nanostruct, 2026; 16(3):3280-3295. DOI: 10.22052/JNS.2026.03.023

INTRODUCTION

Schiff Bases have been of great interest to researchers and scientists in recent years. The large number of Schiff-base ligands used today is due to their high coordination properties and as a result, they can create many different types of structures with metal ions. This diversity in structure allows for a variety of potential applications [1]. The formation of these ligands occurs during a condensation reaction between a primary amine and a carbonyl compound forming an imine or azomethine (C=N) functional group [2]. The azomethine group present in Schiff Bases provides for a highly efficient ligand system allowing for the coordination of metal ions to produce coordination compounds exhibiting notable biological activity, including antibacterial, anticancer, and antifungal effects [3-6]. There has been a considerable amount of interest in Schiff Base ligands derived from oximes due to the vast array of potential applications. Diacetyl monoxime serves as a prevalent and versatile precursor

* *Corresponding Author Email: emanjabar973@gmail.com*

for the synthesis of multidentate Schiff base ligands. Due to the presence of both oxime and carbonyl groups on diacetyl monoxime, it allows for coordination with metal ions to form stable coordination compounds [7]. In addition, diacetyl monoxime can also be used in combination with thiosemicarbazide to detect trace amounts of urea in the presence of other nitrogen containing compounds [8]. Additionally, it has industrial applications as colorless dyes that can be converted into colored compounds [9]. Ag(I) complexes derived from Schiff bases and oximes represent an important area in coordination chemistry due to their diverse applications in biological and industrial fields. These complexes have demonstrated the ability to inhibit the evolution of cancer cells through interaction with DNA and the disruption of enzymes responsible for cell proliferation, making them promising candidates for chemotherapy [10]. They are also used in sensing systems and in silver-coated medical devices for infection prevention [11].

MATERIALS AND METHODS

Chemicals

All materials used were produced by reliable companies and were of high purity. These include: Diacetyl monoxime (BDH), 2-Aminonicotinaldehyde (Macklin), 5-Aminoindole (Merck), Glacial Acetic Acid (Sigma-Aldrich), $AgNO_3$ (Merck), Absolute Ethanol (RCI Labscan), thin-layer chromatography (TLC).

Measurements and Instruments

The structure of the synthesized products was characterized by means of several analytical methods. Vibrational modes were identified through the use of a Shimadzu 8400s FT-IR spectrometer using KBr discs to scan in the 400-4000 cm^{-1} range. Nuclear Magnetic Resonance studies were conducted through the recording of ^{1}H and ^{13}C NMR spectra with a 400 MHz instrument, utilizing DMSO-d_6 as the solvent and TMS as the internal standard for calibration. Elemental Composition (C, H, N) was quantitatively analyzed by a EuroEA3000 CHN-O analyzer. The Physical Property of the melting point was also determined using a Stuart Melting Point Apparatus. The molar conductivities were determined by means of a portable Chinese made instrument model (E-1 Portable Jinan Runjie); magnetic susceptibility measurements by means of an Auto instrument. The electronic transition is studied by obtaining the UV-Vis Absorption Spectra at wavelengths from 200 – 1000 nm with a Shimadzu spectrophotometer in order to obtain information about the molecular transition. The molecular mass is determined by acquiring mass spectra on an AB SCIEX 3200 Q TRAP System. The crystalline form of the substance is evaluated by acquiring the x-ray powder diffraction (xrd) pattern with a D2 Phaser Bruker AXS GmbH diffractometer. TGA studies were conducted utilizing a NETZSCH STA 409 PC Luxx thermobalance under inert argon atmospheres; finally, a ZEISS Sigma FE-SEM was

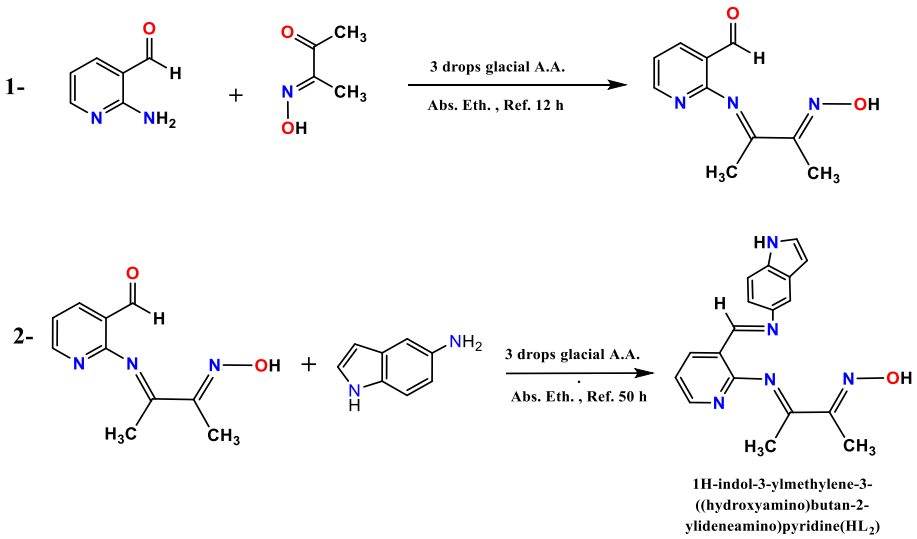

Fig. 1. Preparation steps of the ligand (VIPIBO).

employed for imaging of selected samples.

Procedure

Preparation of the (IVPIBO) Ligand

The total synthesis of target ligand IVPIBO was completed using the multi-step process described in Fig. 1. The first of these steps is the generation of intermediate A, which can be generated through the reaction of diacetyl dioxime (1.011 g) and 2-aminonicotinaldehyde (1.221 g) in equivalent molar amounts (each 0.01 mole) in 25 ml of anhydrous ethanol. Prior to combining the aldehyde solution with the dioxime solution, the aldehyde solution is treated with 3 drops of glacial acetic acid to create acidic conditions. Once the two solutions are mixed, the reaction is placed under reflux for approximately 12 hours with TLC monitoring of the reaction until all of the starting materials have been consumed. Once cooled, the yellow precipitate of intermediate compound A is filtered, washed with anhydrous ethanol to purify it, dried and weighed to afford a 92% yield.

In the next step, intermediate compound A is reacted with 5-aminoindole (1.321 g; 0.01 mole) to generate the final ligand IVPIBO. Both compounds are dissolved in 25 ml of anhydrous ethanol. The solution of compound A is also treated with glacial acetic acid. The reaction mixture is then once again refluxed until the periodic sampling of the reaction indicates that the reaction is complete. The resulting black solid is then cooled, dried and isolated by filtration. Finally, the resulting black crystalline powder of IVPIBO is generated by recrystallizing the black solid from anhydrous ethanol.

Preparation of the Complexes

The Ag(I) complex was made at a 1:1 mole ratio as a 10 ml solution of 0.001 M ethanol, 0.319g IVPIBO (ligand) and 0.001M ethanol, 0.169g AgNO3, with each being mixed together in a 1:1 ratio. The solution was refluxed for 2 hours; then it was allowed to cool down. Black metal ion complex precipitation was achieved after collecting and recrystallizing the resulting precipitate using 100% ethanol.

MTT Assay for Cell Viability

The A549 cell line studied was obtained from the Iranian National Cell Bank located within the Pasteur Institute of Iran. Cells were grown in RPMI-1640 medium (Gibco) with 10% fetal bovine serum (FBS), as well as 100 units/mL of penicillin and 100 micrograms/mL of streptomycin added to the medium. Cultures were kept in a humidified incubator at 37°C and 5% CO_2 in an atmosphere. For regular passage of cultures, cells were washed with PBS and loosened with a trypsin/EDTA (Gibco).

Cell Viability Assay Using MTT

Cell viability was measured using the MTT assay [3-(4,5-Dimethylthiazol-2-yl)-2,5-Diphenyltetrazolium Bromide]. First, A549 cells were treated with trypsin to remove them from culture surfaces. Then they were enumerated and placed in 96-well plates at a density of 1.4×10^4 cells/well in 200 µL of new growth media. Plates were then allowed to incubate for 24 hours to allow the cells to attach to the plate surface and to establish monolayers. At that time the cells were exposed to test compounds made up as stock solutions in DMSO at concentration ranges of 7.4 to 600 µg/mL. Cells that had been treated with the test compounds were incubated for an additional 24 hours under standard laboratory conditions (37°C, 5% CO_2), along with untreated controls. Following the treatment period, the growth media was removed from all wells and 200 µL of MTT solution (0.5 mg/mL in PBS) was added to each well. Incubation continued for four hours. At that time the MTT solution was removed from each well and the intracellular formazan was solubilized by the addition of 100 µL of DMSO. Absorbance measurements were obtained from each well at 570 nm on a BioTek Wave XS2 ELISA Microplate Reader. Dose response curves were generated to obtain IC50 values from the data collected [12,13].

DPPH Assay for Antioxidant Activity

Antioxidant ability of the synthesized ligand and its Ag(I) complex was assessed by employing the 2,2-diphenyl-1-picrylhydrazyl (DPPH) free radical scavenging assay. Ascorbic acid was used as a reference compound for comparative purposes. Ethanolic solutions of the ligand, the complex, and ascorbic acid were made up at concentrations of 500, 1000, 1500, 2000, and 2500 µg/mL. An aliquot of 0.3 mL from each sample concentration was combined with 2.5 mL of an ethanolic DPPH solution for the assay. The solutions were then allowed to incubate in the dark for thirty minutes to allow for the completion of the scavenging reaction. After incubation, the loss

of DPPH was determined through measurement of the loss of absorbance at 517 nm via a UV/vis spectrophotometer. The % of radical inhibited was subsequently determined utilizing the previously stated equation [14,15]:

$$\% \text{ Inhibition} = \frac{\text{Absorbance of control} - \text{Absorbance of sample}}{\text{Absorbance of control}} \times 100 \quad (1)$$

RESULTS AND DISCUSSION

A novel Schiff-base ligand (IVPIBO), was produced using a two step process that involved the combination of diacetylmonoxime, 2-aminonicotinaldehyde and 5-aminoindole, to produce IVPIBO, as reported earlier. An alcoholic solution of the ligand was mixed with an equivalent amount of $AgNO_3$ to prepare the silver (I) complex. Elemental Analysis (C, H, N), Flame Atomic Absorption Spectroscopy (for metals) and determination of metal content in the complex was used to verify the empirical formula of the ligand and the Ag(I) complex as well as confirm that the complex had a 1:1 metal-to-ligand ratio as indicated in the structure of the complex as shown in Table 1, and the results confirmed the calculated and theoretical information for both the metal content and the chemical composition of the complex.

^{1}H, ^{13}C- NMR Spectra of the Ligand (IVPIBO)

The structure of the IVPIBO ligand was determined through the use of ^{1}H and ^{13}C NMR data; the NMR data were acquired in DMSO-d6 solution with TMS as an internal reference. The ^{1}H NMR data showed five different chemical environments. The hydroxyl proton of the oxime functional group (N-OH), which is characterized by a singlet that appears at a downfield position relative to TMS (δ 12.3 ppm)[16], and the N-H proton of the indole ring system, which appeared as a singlet at a lower field than TMS (δ 11.1 ppm) [17], are two significant signals. A Singlet at δ = 8.7 ppm,1H is the Azomethine (CH=N) Proton[18]; a Signal at δ = 1.8 ppm,3H (19) are Methyl Protons of the CH_3-N(OH) Group; a Signal at δ = 2.3 ppm,3H

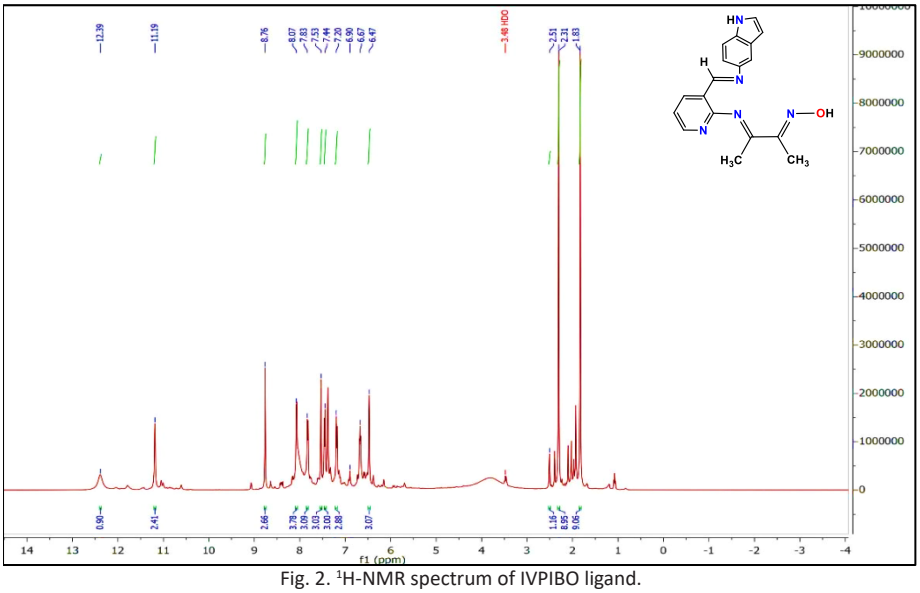

Fig. 2. ^{1}H-NMR spectrum of IVPIBO ligand.

Table 1. Analytical characteristics of the Ag(I) complex and its ligand.

Compound (Chemical Formula)	Color	M.P (^{0}C)	Yield %	M. Wt. (g/mole)	Calc. (Found)%			
					C	H	N	M
Ligand (IVPIBO) $C_{18}H_{17}N_5O$	Black	87-91	90	319.36	67.69 (66.73)	5.36 (5.29)	21.93 (20.87)	- -
$[Ag(IVPBO)NO_3]$ $C_{18}H_{17}N_6O_4Ag$	Black	183-185	91	489.23	44.19 (43.84)	3.50 (3.42)	17.18 (16.09)	22.04 (22.21)

are Methyl Protons of the Azomethine Moiety[19]. Signals in the Aromatic Region are due to the Benzene Ring Protons (δ = 6.4-8 ppm, 8H); see the ^{1}H-NMR Spectrum of IVPIBO Ligand in Fig. 2.

The ^{13}C- NMR spectrum of the IVPIBO ligand displayed several characteristic signals. A resonance at 142 ppm corresponds to the aromatic carbon C1, which is bonded to the nitrogen atom of the indole five-membered ring [20]. Signals appearing in the range of 150–164 ppm were assigned to the azomethine carbon [21] and to carbons adjacent to nitrogen atoms, specifically C16, C15, C13, C12, and C9.Two additional signals at 25 ppm and 8.4 ppm were attributed to the terminal methyl carbons C17 and C18, which are not bonded to nitrogen. Within the 102-143 ppm range, many signals corresponding to aromatic ring carbons were detected. In the DMSO solvent, the carbon atoms give rise to a peak at 40 ppm. Fig. 3 displays the IVPIBO ligand's ^{1}C NMR spectrum.

The mass spectrum of the IVPIBO ligand

Mass spectrometry has been used to confirm the chemical structural integrity of the IVPIBO ligand that was synthesized. A fragmentation pattern for the mass spectrum shown in Fig. 4, is completely consistent with the molecular structure as proposed; and the molecular ion peak [M]+ was detected at an m/z value of 319.9. This experimental m/z value of 319.9 agrees well with the theoretical molar mass of the empirical formula C16H18N5O of 319.37 g/mole, thus validating the composition of the ligand. A base peak was observed at m/z = 237.1. Table 2 and Fig.

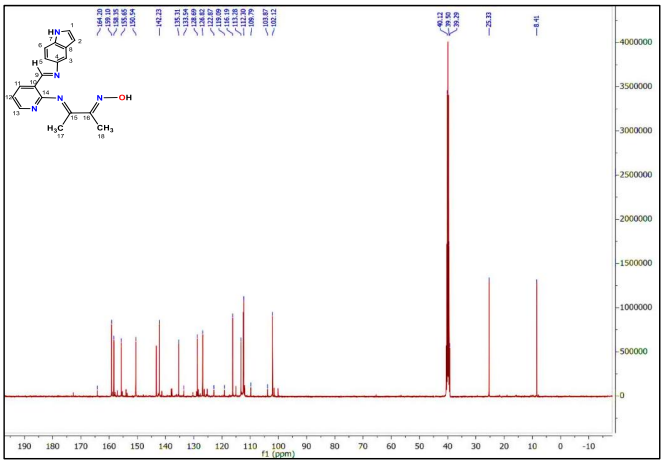

Fig. 3. ^{13}C NMR spectrum of the IVPIBO ligand.

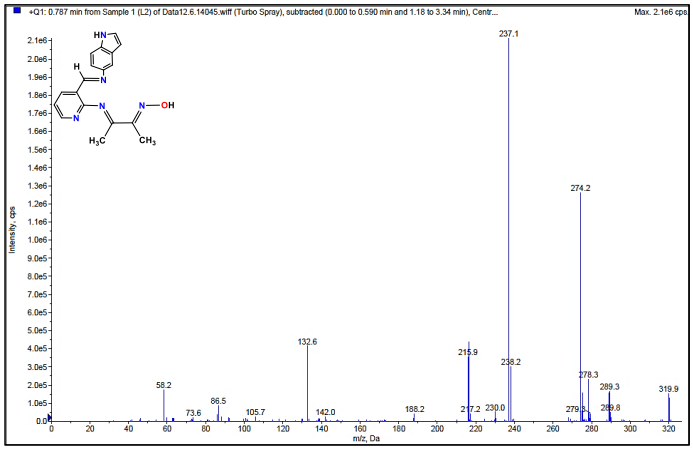

Fig. 4. Mass spectrum of IVPIBO ligand.

5 illustrate the mass fragmentation pathways and the resulting fragments of this ligand.

The mass spectrum of the Ag(I) complex

Fig. 6 shows that the primary molecular ion peak at (m/z = 489.25) is absent from the mass spectrum of the Ag(I) complex. This reveals that the complex is unstable in the mass spectrometer and undergoes fragmentation before reaching the detector [22]. Instead, a major peak appeared at (m/z = 360) corresponding to the fragment $[C_{18}H_{12}N_6O_3]$ after the loss of the silver atom and additional parts. Several other peaks also appeared at different m/z values, as listed in Table 3. Fig. 7 illustrates the mass fragmentation pathways of the complex.

FT-IR Spectrum

The FT-IR spectrum for the ligand showed multiple absorption bands that could be assigned based on the molecular structure. A wide band from 3200 to 3450 cm^{-1} represents the overlap of the O-H from the oxime group and the N-H from the indole group[23]. Bands near 3030 cm^{-1}

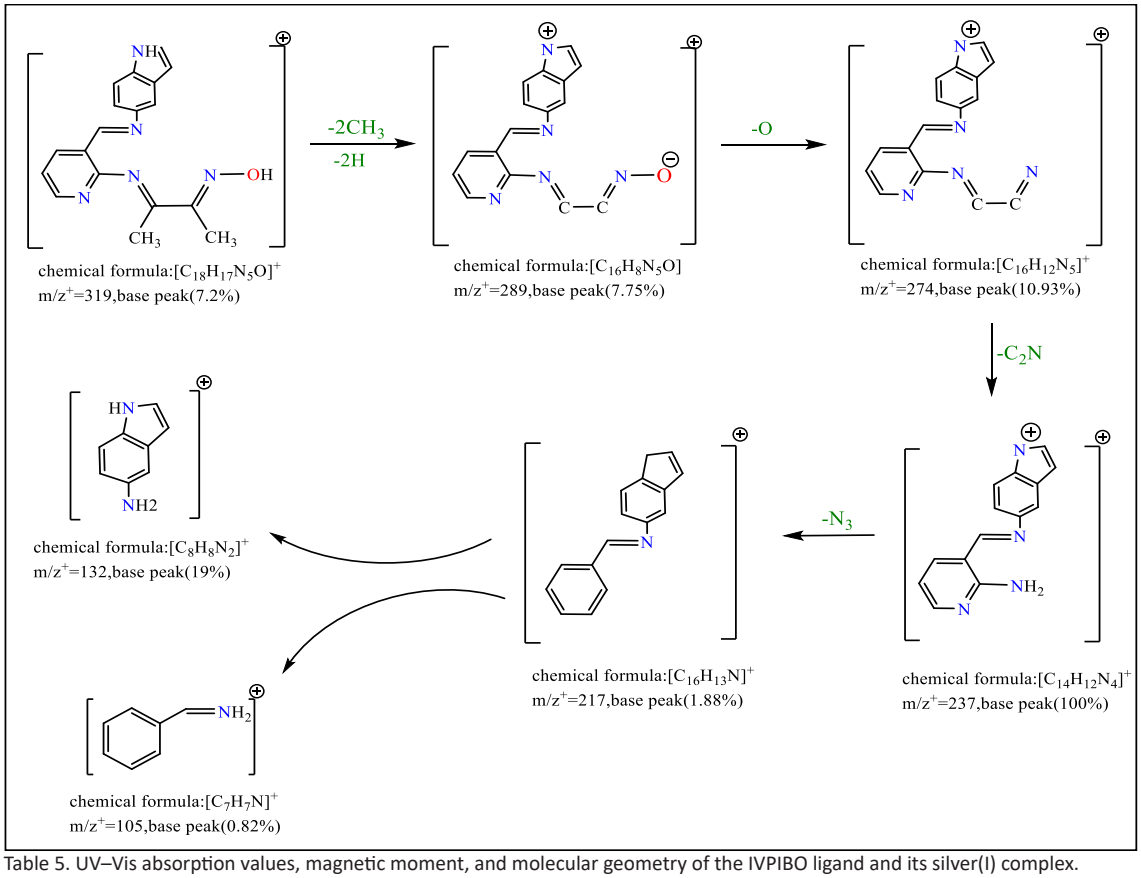

Table 5. UV–Vis absorption values, magnetic moment, and molecular geometry of the IVPIBO ligand and its silver(I) complex.

Table 2. Mass fragmentation products of the IVPIBO ligand.

Fragment	m/z⁺ Exact	Relative Abuondance(%)
$[C_{18}H_{17}N_5O]^+$	319	7.2
$[C_{16}H_{11}N_5O]^+$	289	7.75
$[C_{16}H_{10}N_5]^+$	278	10.93
$[C_{14}H_{12}N_4]^+$	237	100
$[C_{16}H_{13}N]^+$	217	1.88
$[C_8H_8N_2]^+$	132	19

represent the C-H bonds from the aromatic portion of the molecule while bands from 2839 to 2972 cm^{-1} are owing to the C-H stretchings from the aliphatic portion of the molecule. The azomethine group in the ligand was identified using the most intense band at 1681 cm^{-1} corresponding to the C=N stretch [24]. The C=N stretch of the oxime group was observed as a band at 1583 cm^{-1}. Bands agreeing to C=C appeared at 1454–1560 cm^{-1}.

In comparison with the free ligand, the addition of bands along with significant changes were detected in the Figure indicating coordination of the metal ion and the ligand. The differences between the infrared spectra of the free ligand and its Ag(I) compound, as illustrated in Tables 4-6 and shown in Figs. 8 and 9 show that the ligand has undergone chemical bonding with the metal ion as evidenced by the change in the positions and intensities of the bands. More specifically, the broad bands associated with the stretching vibrations of the hydroxyl and amine groups on the ligand are replaced with a relatively sharp but lower intensity band, at approximately 3103–3209 cm−1, in the IR spectrum of the complex, indicating that the oxime and indolene nitrogen atom are involved in bonding with the metal ion.

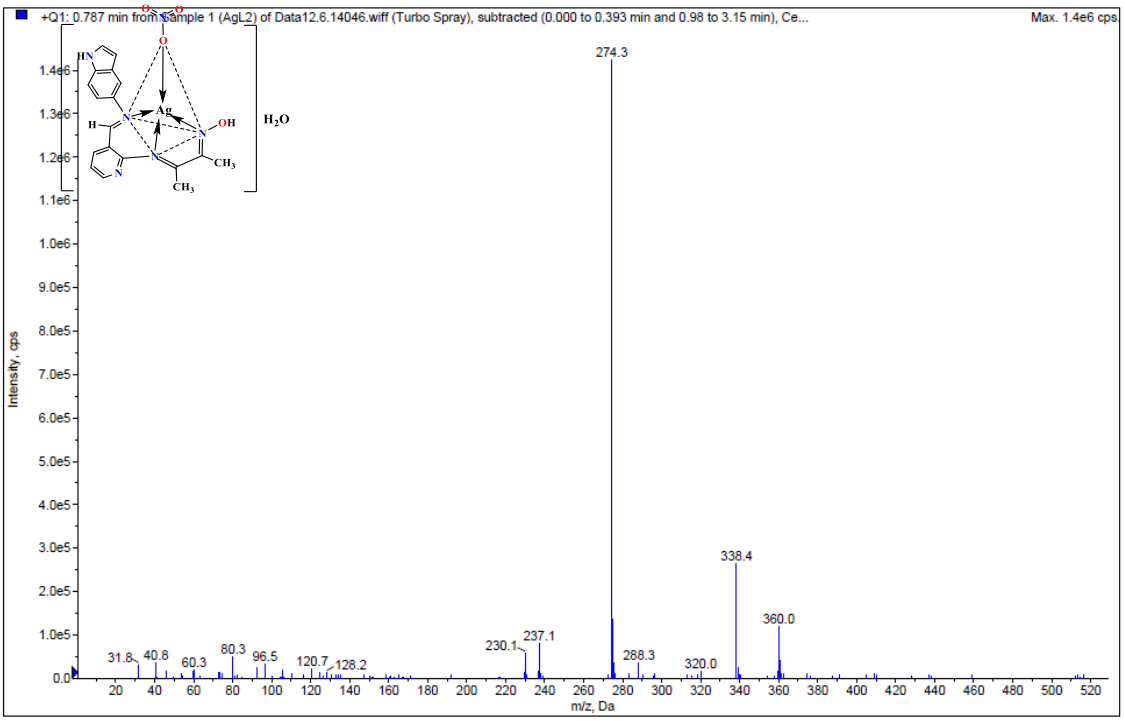

Fig. 6. Mass spectrum of Ag(I) Complex.

Table 3. Mass fragmentation products of the Ag(I) Complex.

Fragment	m/z^+ Exact	Relative Abuondance(%)
$[Ag(C_{18}H_{17}N_6O_4)]^+$	489.25	0
$[C_{16}H_{12}N_6O_3]^+$	360	3.5
$[C_{16}H_{16}N_6O_3]^+$	338	6.5
$[C_{16}H_{12}N_6O_2]^+$	320	1
$[C_{16}H_{12}N_5O]^+$	288	1.4
$[C_{16}H_{10}N_4O]^+$	274	100
$[C_{14}H_{11}N_3]^+$	237	4.5
$[C_{14}H_{20}N_3]$	230	3.0
$[C_8H_{15}N]$	128	0.8
$[C_6H_8N_2]$	108	0.5

A new band corresponding to an expected band for the NO stretching vibration of a coordinated nitrate group appears at 1749 cm−1. In addition, the C=N stretching vibration shifts to higher wavenumbers and occurs at 1662 cm^{-1} in the complex (approximately +19.29 cm^{-1} from the free ligand), which is an indication of C=N coordination; this is a well established method for determining coordination. The presence of the complex was also indicated by the presence of additional

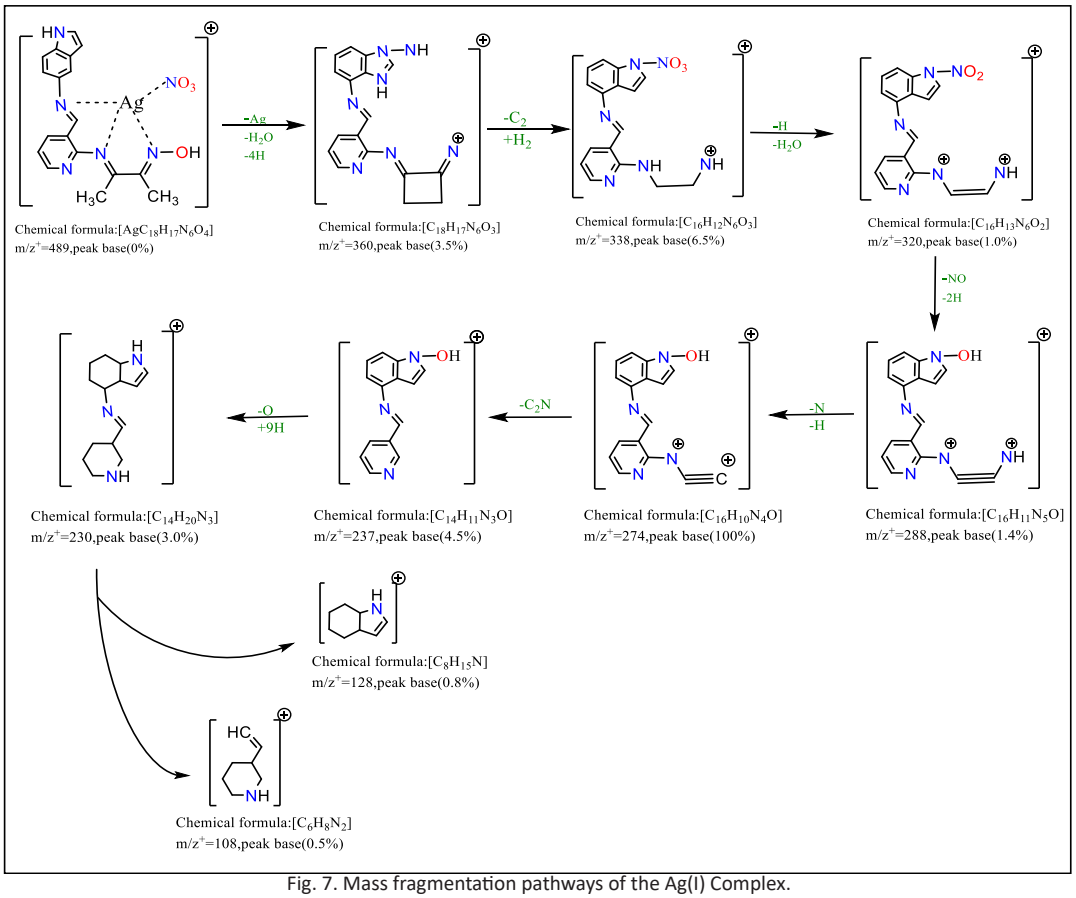

Fig. 7. Mass fragmentation pathways of the Ag(I) Complex.

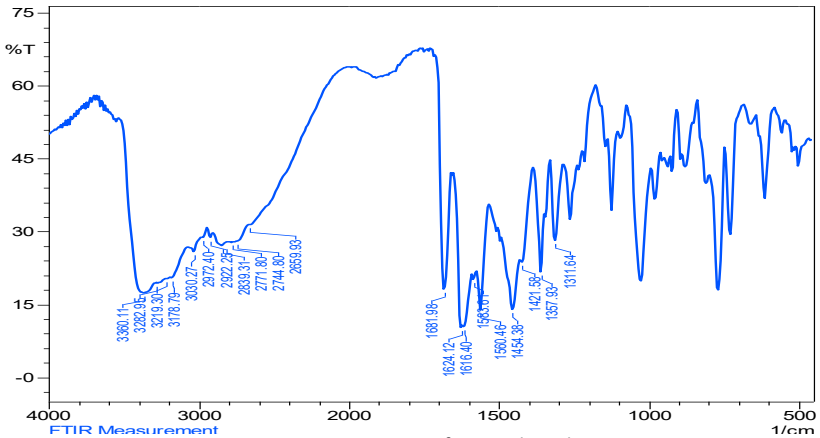

Fig. 8. FT-IR spectrum of IVPIBO ligand.

bands in the low frequency range at 549–609 cm^{-1} and 428–466 cm^{-1}, which corresponded to the stretching vibrations of M-N and M-O bonds [25].

Electronic Spectra

The electronic absorption spectra of the free ligand and its Ag(I) complex were collected to determine their electronic properties. Their results are presented in Table 5 and Fig. 10. The free ligand exhibited three absorption bands. The two strong absorption bands at 233 nm and 265 nm were due to π → π* transitions that occurred in the aromatic pyridine ring and the aromatic indole ring. The least intense band at 302 nm was due to n → π* transitions that occurred because of the non-bonded electron pairs of the azomethine group and the oxime group[26]. When Ag(I) is added to the free ligand, the electronic absorption spectrum shows some changes in comparison to the free ligand's spectrum. The intra-ligand transitions show very little shift (at approximately 219 nm, 254 nm, and 300 nm). The most

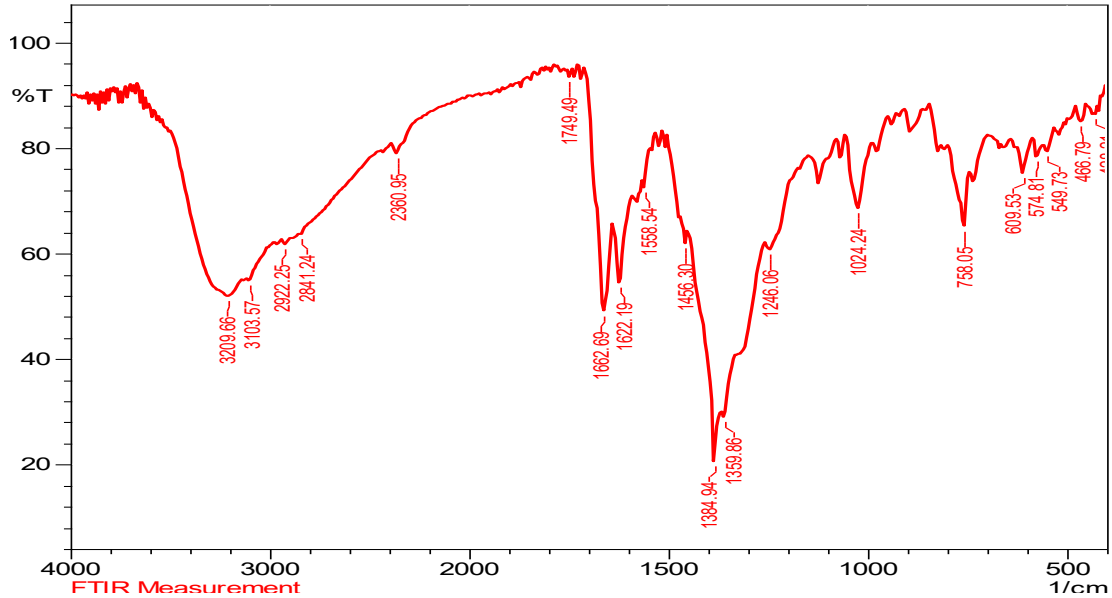

Fig. 9. FT-IR spectrum Ag(I) Complex.

Table 4. FT-IR absorption bands of the ligand and its complex.

Compound	υ ((O-H) Oxime υ(N-H)I ndole	υ(C-H) arom.	υ(N=O) Nitrate	υ(C=N) Imine	υ(C=C) arom.	υ(M-N) υ(M-O)
IVPIBO-Ligand	3200-3450	3030	------	1681	1454-1560	------
Ag(I)-Complex	3103-3209	3103	1749	1662	1456-1568	549-609 428-466

Table 5. UV–Vis absorption values, magnetic moment, and molecular geometry of the IVPIBO ligand and its silver(I) complex.

Compounds	λ (nm)	υ (cm^{-1})	Transitions	μeff (B.M)	Geometry
Ligand (IVPIBO) $C_{17}H_{18}N_5O$	233	42918	π-π*	-	-
	265	37735	π-π*		
	302	33112	n-π*		
[Ag(IVPIBO)] $C_{17}H_{18}N_6O_4Ag$	219	45662	Ligand field	(Dia.)	sp^3 tetraheadral
	254	39370	Ligand field		
	300	33333	Ligand field		
	393	25445	MLCT		

significant difference is the presence of a new, broad, low energy shoulder at 393 nm which is characteristic of a metal-to-ligand charge transfer (MLCT) transition, therefore confirming there is an electronic interaction occurring between the silver ion and the ligand. The magnetic susceptibility measurements on the Ag(I) complex also support this assertion, since they indicate that the complex is diamagnetic; therefore, it has no net magnetic moment. Since the complex is diamagnetic and the spectral evidence along with previous reports of silver complexes [27)] support a tetrahedral geometry about the Ag(I) center, this is the assumed geometry of the complex.

Determination of the Metal-to-Ligand Ratio

Using the absorbance of each of a series of IVPIBO ligand solutions at the maximum wavelength (λmax), the molar ratio [M:L] of the ligand to the Ag(I) ion in solution was determined. The same amount of metal ion was added to each solution. The molar ratio (VM / VL) of the metal to ligand and the resulting absorbance value for each of the solutions are presented as follows. The point of intersection of the two lines obtained from the linear fit to these data will determine the metal-to-ligand ratio. The data obtained and depicted in Fig. 11 indicate an molar ratio of [1:1].

Molar Conductivity

A molar conductivity of (16.00 $S \cdot cm^2 \cdot mol^{-1}$) for Ag(I) complex at ($10^{-3}$ M) at room temperature has been measured. As this molar conductivity is very low, it is indicative that the complex is not electrolytic, i.e. not ionic in character. The absence of nitrate ions from outside the coordination sphere leads to the formation of a neutral entity with no electrical charge [28].

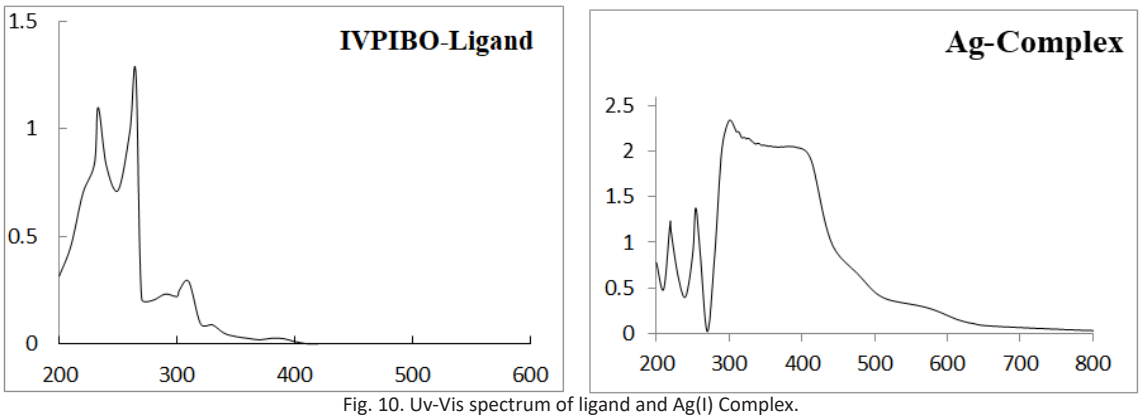

Fig. 10. Uv-Vis spectrum of ligand and Ag(I) Complex.

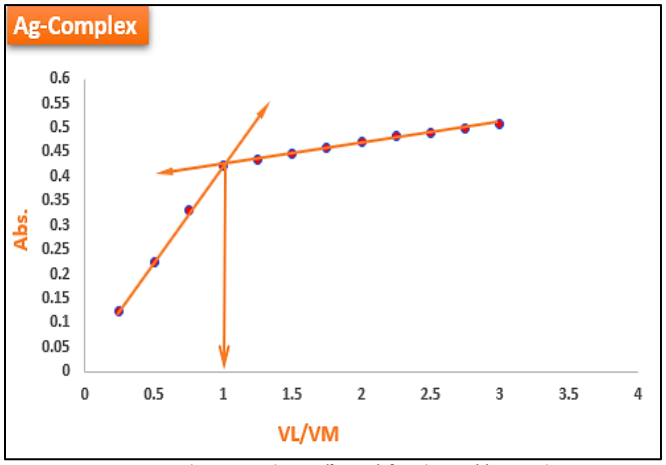

Fig. 11. Molar ratio plot at (λmax) for the Ag(I) complex.

X-ray Diffraction Analysis

X-ray Diffraction (XRD) Analysis was used to study the Ligand and its Ag(I)-ligand Complex (See Fig. 12). Average crystallite sizes were determined for the ligand and the Ag(I)-ligand Complex using the Debye-Scherrer Equation, as well as the corresponding diffraction patterns at 2θ = 5°–80°. The ligand and Ag(I)-ligand Complex had average crystallite diameters of 43.25 nm and 92.16 nm respectively. These measurements confirm that both synthesized materials are indeed in the nanometer scale [29].

Field Emission Scanning Electron Microscopy (FE-SEM) Analysis

The FE-SEM analysis of the IVPIBO ligand and the Ag(I) complex, shown in Fig. 13, revealed that the ligand exhibits a somewhat rod-like morphology. Using the ImageJ software, the average particle size was calculated to be (21.07) nm. In contrast, the FE-SEM images of the Ag(I) complex showed that most of its particles are spherical and non-

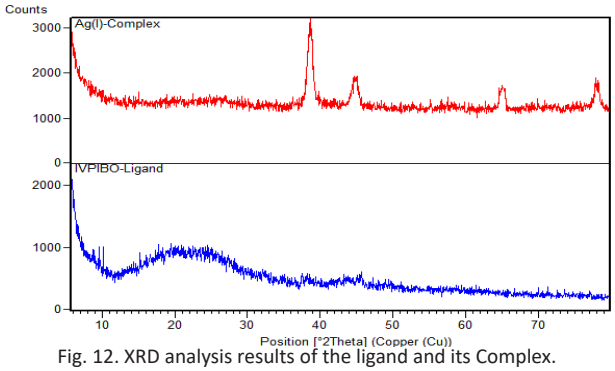

Fig. 12. XRD analysis results of the ligand and its Complex.

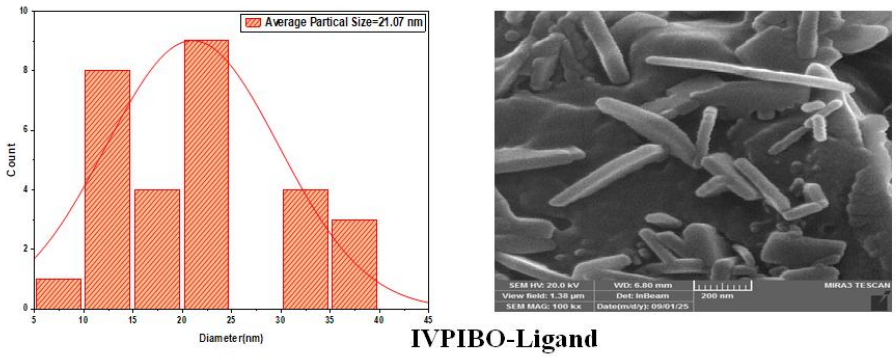

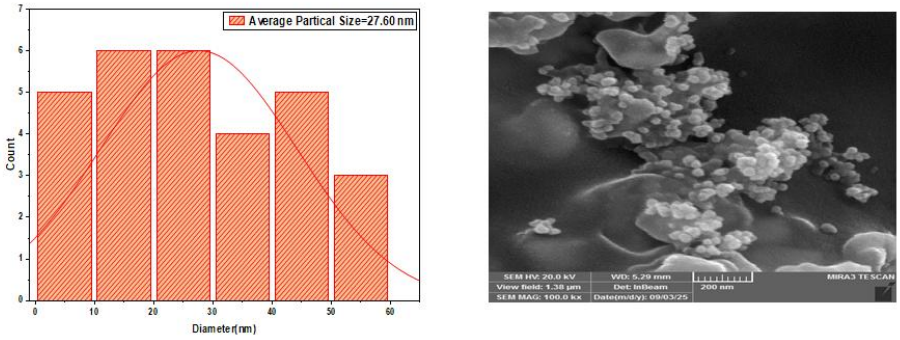

Fig. 13. FE-SEM Images of ligand and Ag(I) complex.

uniform, with an average particle size of (27.60) nm. These findings indicate that both the ligand and its complex possess crystalline and granular structures, which is consistent with the XRD results. Therefore, the ligand and its complex fall within the nanoscale range [30].

Thermogravimetric Analysis (TG-DTG) of IVPIBO Ligand and Ag(I) Complex

Both the IVPIBO ligand and its silver (I) complex decomposed in three steps during thermogravimetric analysis (TG/DTG) as presented in Fig 14 and shown in detail in Table 6. This was accomplished with the sample heated at a 10°C/min rate up to 620°C in a nitrogen-free argon environment and a nearly complete decomposition of both materials occurred at the conclusion of the heat treatment cycle permitting the identification of the individual thermal degradation stages of each material.

Antioxidant Activity

The DPPH free radical scavenging assays displayed that both IVPIBO, the synthesized ligand, and its Ag(I) complex exhibit a concentration dependent effect on antioxidant activity. The inhibitory percent for IVPIBO and the Ag(I) complex at the highest concentration used in this study (2500) µg/mL were approximately (63.6)% and (61.5)% respectively. At the lower concentrations studied, the Ag(I) complex was slightly more effective than the ligand, as indicated by its inhibitory percent being approximately (45.2)% at (500) µg/mL versus (43.1)% for the ligand. The antioxidant activity shown by IVPIBO and the Ag(I) complex can be assigned to their ability to quench the DPPH radical through hydrogen atom abstraction, as illustrated in Fig. 15, where the purple colored radical is converted to the colorless, non-radical form (DPPH-H)[31]. The inhibition percentages of the ligand and complex

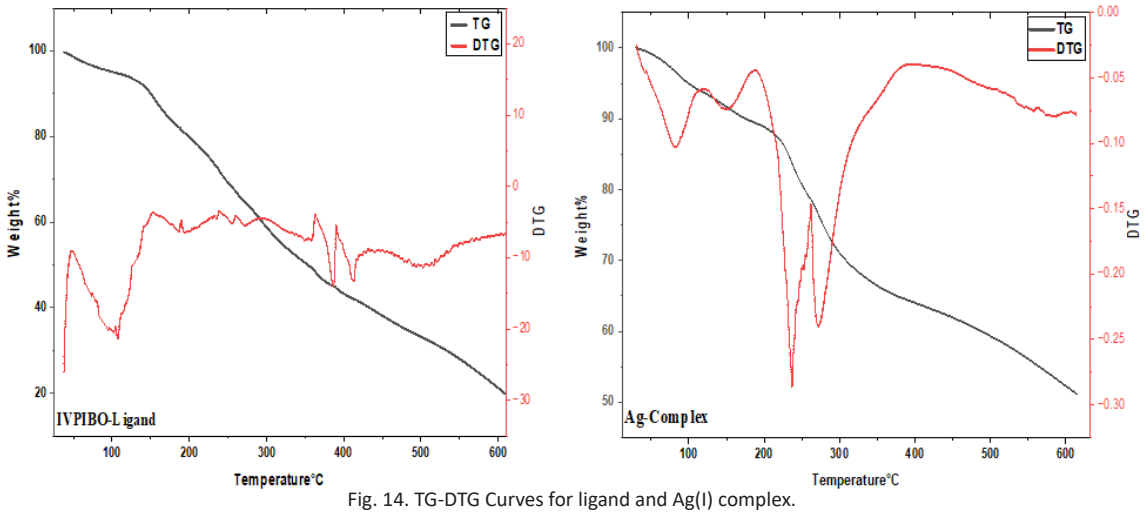

Fig. 14. TG-DTG Curves for ligand and Ag(I) complex.

Table 6. Thermogravimetric decomposition data of the IVPIBO ligand and its Ag(I) complex.

Compound	Dissiciation steps	Temperatuer range °C	Mass loss%	DTG peak°C	Decomposition Assignment
IVPIBO-Ligand $C_{17}H_{18}N_5O$	1st step	31.99-122.49	6.15	120	Loss of water and solvent
	2nd step	122.49-320.92	39.06	240	N-OH,C=N,CH_3 Loss of
	3rd step	320.92-614.04	35.76	400	Loss of pyridine and benzene derivatives
	Residue	>614.04	19.03	--------	Carbonaceous residue
Ag-Complex $[C_{17}H_{18}N_6O_4Ag]$	1st step	34.88-185.96	10.49	90	Loss of water and cleavage of Ag-L bond
	2nd step	185.96-369.71	24.32	230	Loss of indole + pyridine rings
	3rd step	369.71-614.66	14.12	370	(C_3H_7N) Loss of (C_2H_6O),
	Residue	>614.66	51.61	------	Inorganic residue such as (Ag_2O)

are presented in Table 7, and graphically depicted in Fig. 16.

Comparing the Ligand's (IVPIBO) Impact on Normal Cell (WRL-68) and Lung Cancer Cell (A549) Growth

Using an MTT assay for 24 h with concentrations of 7.4 to 600 µg/mL, we evaluated the in vitro anticancer effects of the ligand IVPIBO on A549 lung cancer cells and WRL-68 normal cells. As shown via the experimental data, both normal and cancer cells exhibited a decrease in viability with increasing drug concentrations. Specifically, viability of cancerous cells dropped from 87.89 % at 7.4 µg/ml to 10.44 % at 600 µg/ml while that of non-cancerous cells dropped from 90.81 % to 51.24 % under the same conditions; therefore, demonstrating a strong and selective inhibitory effect on growth of cancer cells. The IC_{50} values for

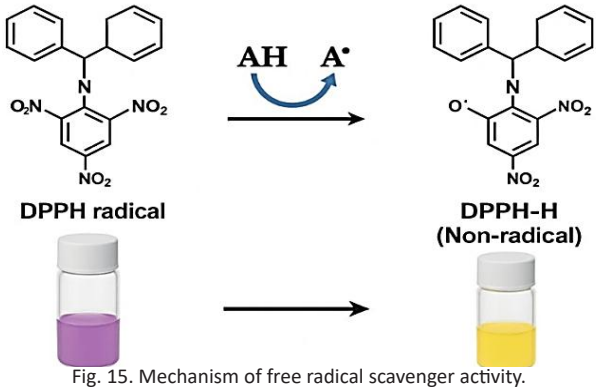

Fig. 15. Mechanism of free radical scavenger activity.

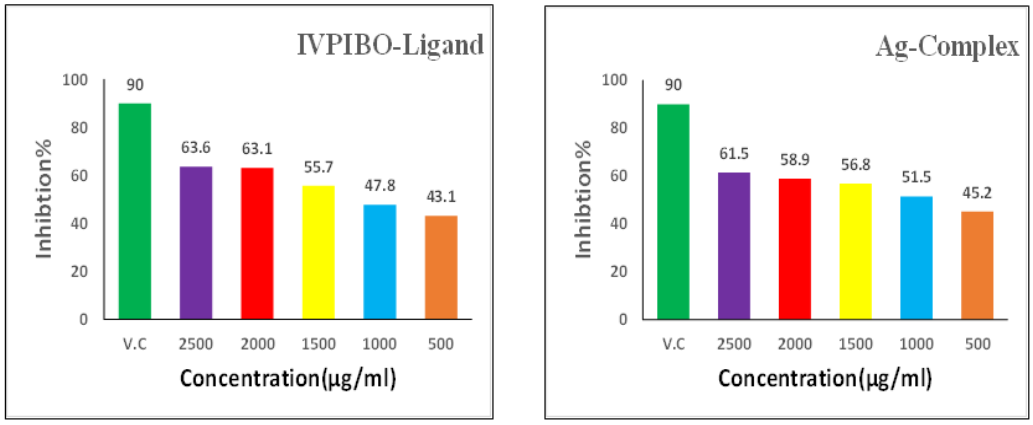

Fig. 16. Antioxidant activity for ligand and complex.

Table 7. Inhibition percentage of IVPIBO ligand and Ag(I) complex with different concentrations.

Conc. µg/ml	IVPIBO-Ligand		Ag(I)-Complex	
	Absorbance	Inhibition percentage	Absorbance	Inhibition percentage
Control	1.9	0 %	1.9	0 %
Ascorbic acid (v.c)	0.18	90 %	0.18	90 %
2500 µg/ml	0.69	63.6%	0.73	61.5 %
2000 µg/ml	0.70	63.1 %	0.78	58.9 %
1500 µg/ml	0.84	55.7 %	0.82	56.8%
1000 µg/ml	0.99	47.8 %	0.92	51.5 %
500 µg/ml	1.08	43.1 %	1.04	45.2 %

both cancerous and normal cells were calculated, as shown in Fig. 17 and Table 8.

Influence of the Ag(I) Complex on the Growth of Lung Cancer Cells (A549) and Normal Cells (WRL-68)

The A(g)(I) complex had a lower level of activity in comparison to the free ligand when examined using both lung cancer cells (A549) and normal lung cells (WRL-68). Normal cells dropped from 87.19% viable down to 56.20% viability with the complex; whereas lung cancer cells dropped from 87.54% viable down to 37.32% viability when exposed to 600 µg/mL of the A(g)(I) complex.

Table 8. Inhibition values of lung cancer cells (A549) and normal cells (WRL-68) treated with the ligand (IVPIBO).

Concentration (µg/ml)	Cancer line cells (A54)			Normal line cells (WRL-68)		
	Cell Viability% Mean	SD	%Cell Inhibition	%Cell Viability Mean	SD	Cell %Inhibition
7.4	87.89	5.21	12.11	90.81	0.15	9.19
22.2	76.05	6.82	23.95	75.41	0.88	24.32
66.6	60.26	2.11	39.74	67.77	2.63	32.23
200	35.61	0.25	64.39	55.17	2.34	44.83
600	10.44	0.87	89.56	51.24	2.63	48.76
IC_{50}	83.67(µg/ml)			246.02(µg/ml)		

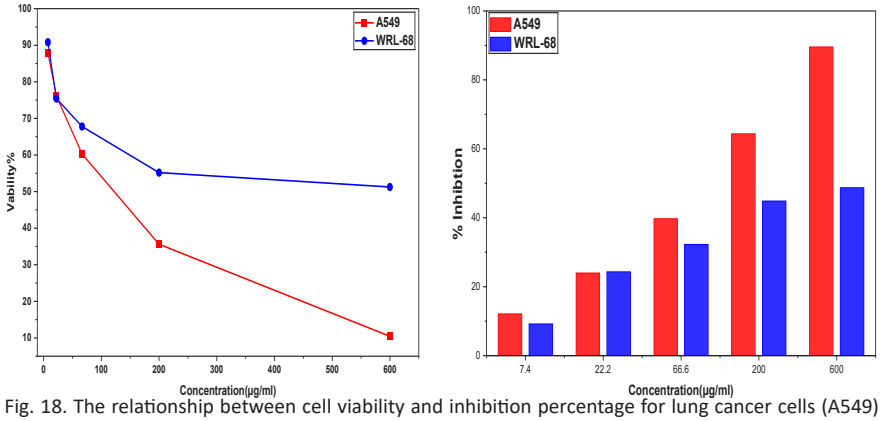

Fig. 18. The relationship between cell viability and inhibition percentage for lung cancer cells (A549) and normal cells (WRL-68) in response to different concentrations of the Ag(I)Complex.

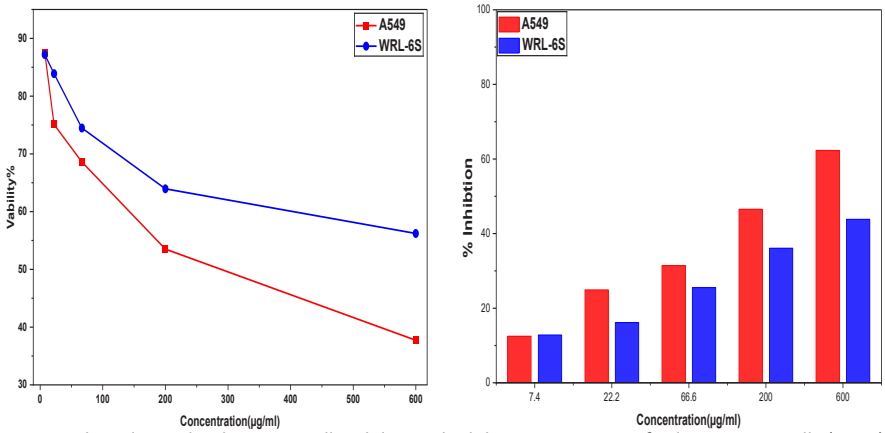

Fig. 19. The relationship between cell viability and inhibition percentage for lung cancer cells (A549) and normal cells (WRL-68) in response to different concentrations of the Ag(I)Complex.

Table 9. Inhibition values for lung cancer cells (A549) and normal cells (WRL-68) treated with the Ag(I) complex.

Concentration (µg/ml)	Cancer line cells A549			Normal line cells WRL-68		
	Cell Viability% Mean	SD	%Cell Inhibition	Cell Viability% Mean	SD	Cell %Inhibition
7.4	87.54	6.20	12.46	87.19	5.26	12.81
22.2	75.09	6.20	24.91	83.88	0.29	16.12
66.6	68.60	1.74	31.4	74.48	10.08	25.52
200	53.51	1.66	46.49	63.95	1.90	36.05
600	37.72	2.23	62.28	56.20	4.68	43.8
IC_{50}	248.15(µg/ml)			742.82(µg/ml)		

These results indicate that the complex exhibits relatively higher cytotoxic activity against lung cancer cells compared to its effect on normal cells. The IC_{50} values for both cancerous and normal cells were calculated, as shown in Fig. 18 and Table 9.

The suggested stereochemical geometry of the complex

Based on the obtained spectroscopic and analytical results regarding the available coordination sites of the ligand and the coordination number of the Ag(I) ion, suggests that the synthesized complex adopts a tetrahedral geometry, as illustrated in Fig. 19.

CONCLUSION

The Schiff Base Ligand (IVPIBO) was successfully synthesized and investigated with respect to its coordination capability toward the silver ion (Ag(I)). The IVPIBO Ligand acted as a tridentate ligand as evidenced from the spectroscopic methods employed for characterization; 1H-NMR, 13C-NMR, FT-IR, UV-VIS, MS, XRD, TG-DTG, elemental analysis (C, H, N), crystallinity (FE-SEM), susceptibility (magnetic), AAS, and molar conductivity. The azomethine group, oxime group and the pyridine ring provide the three nitrogen donor atoms which bind to the Ag(I) center while the fourth site is occupied by the nitrate anion (O-NO2). This results in a tetrahedral geometry being adopted by this complex. Employing ascorbic acid as a standard, the antioxidant potential of both the ligand and its complex was determined through the DPPH free radical scavenging method. Biological activity tests were also conducted using lung cancer (A549) and normal cells (WRL-68). These tests measured the ligands' and complexes' effects on the survival of the cells and their cytotoxic effects in comparison to one another. In comparison to A549 cancer cells, the ligand displayed greater activity than the silver complex. Therefore, there is evidence that the ligand may have utility as a therapeutic agent for various uses.

CONFLICT OF INTEREST

The authors declare that there is no conflict of interests regarding the publication of this manuscript.

REFERENCES

1. Marinova PE, Tamahkyarova KD. Synthesis, Investigation, Biological Evaluation, and Application of Coordination Compounds with Schiff Base—A Review. Compounds. 2025;5(2):14.
2. Borisova NE, Reshetova MD, Ustynyuk YA. Metal-Free Methods in the Synthesis of Macrocyclic Schiff Bases. Chem Rev. 2006;107(1):46-79.
3. Li X, Bi C-f, Fan Y-h, Zhang X, Meng X-m, Cui L-s. Synthesis, crystal structure and anticancer activity of a novel ternary copper(II) complex with Schiff base derived from 2-amino-4-fluorobenzoic acid and salicylaldehyde. Inorg Chem Commun. 2014;50:35-41.
4. Pradeepa SM, Bhojya Naik HS, Vinay Kumar B, Indira Priyadarsini K, Barik A, Ravikumar Naik TR. Cobalt(II), Nickel(II) and Copper(II) complexes of a tetradentate Schiff base as photosensitizers: Quantum yield of 1O2 generation and its promising role in anti-tumor activity. Spectrochimica Acta Part A: Molecular and Biomolecular Spectroscopy. 2013;101:132-139.
5. li P, Niu M, Hong M, Cheng S, Dou J. Effect of structure and composition of nickel(II) complexes with salicylidene Schiff base ligands on their DNA/protein interaction and cytotoxicity. J Inorg Biochem. 2014;137:101-108.
6. Nabhan KJ, Mahdi AS, Al-Zaidi BH, Ismail AH, Nasif ZN. New Tetra-dentate Schiff Base Ligand N2O2 and Its Complexes with Some of Metal Ions: Preparation, Identification, and Studying Their Enzymatic and Biological Activities. Baghdad Science Journal. 2022;19(1):0155.
7. Gupta BD, Singh V, Yamuna R, Barclay T, Cordes W. Organocobaloximes with Mixed Dioxime Equatorial Ligands: A Convenient One-Pot Synthesis. X-ray Structures and Cis−Trans Influence Studies. Organometallics. 2003;22(13):2670-2678.
8. Douglas LA, Bremner JM. Colorimetric Determination of Microgram Quantities of Urea. Anal Lett. 1970;3(2):79-87.
9. Mostafa MM, Elaskalany AH, El-Kkholy DE. Single crystal X-ray of 1-[(1,2,4-triazole-4-yl)imino]diacetyl monoxime (L)

as a novel triazole and the characterization and biological studies of its chelates of Co^{2+}, Pd^{2+}, and Fe^{3+}. Appl Organomet Chem. 2020;34(9).
10. Chernousova S, Epple M. Silver as Antibacterial Agent: Ion, Nanoparticle, and Metal. Angew Chem Int Ed. 2012;52(6):1636-1653.
11. Hebeish A, El-Rafie MH, El-Sheikh MA, Seleem AA, El-Naggar ME. Antimicrobial wound dressing and anti-inflammatory efficacy of silver nanoparticles. Int J Biol Macromol. 2014;65:509-515.
12. Hu M, Yang J. Down-regulation of lncRNA UCA1 enhances radiosensitivity in prostate cancer by suppressing EIF4G1 expression via sponging miR-331-3p. Cancer Cell International. 2020;20(1).
13. Mosmann T. Rapid colorimetric assay for cellular growth and survival: Application to proliferation and cytotoxicity assays. J Immunol Methods. 1983;65(1-2):55-63.
14. Liang N, Kitts D. Antioxidant Property of Coffee Components: Assessment of Methods that Define Mechanisms of Action. Molecules. 2014;19(11):19180-19208.
15. Hoang AS, Tran TH, Nguyen HN, Vu HS, Vo TP, Phan C, et al. Synthesis of oxime from a renewable resource for metal extraction. Korean J Chem Eng. 2015;32(8):1598-1605.
16. Rangappa MM, Keshavayya J, Murali Krishna P, Rajesh K. Transition metal complexes of ligand 4-imino-3-[(4,5,6,7-tetrahydro-1,3-benzothiazol-2-yl)diazenyl]-4H pyrimido[2,1-b][1,3]benzothiazol-2-ol containing benzothiazole moiety: Synthesis, spectroscopic characterization and biological evaluation. Inorg Chem Commun. 2021;127:108524.
17. Maddila S, Gorle S, Seshadri N, Lavanya P, Jonnalagadda SB. Synthesis, antibacterial and antifungal activity of novel benzothiazole pyrimidine derivatives. Arabian Journal of Chemistry. 2016;9(5):681-687.
18. Al-Shamry AA, Khalaf MM, El-Lateef HMA, Yousef TA, Mohamed GG, El-Deen KMK, et al. Development of New Azomethine Metal Chelates Derived from Isatin: DFT and Pharmaceutical Studies. Materials. 2022;16(1):83.
19. Rosnizam AN, Hamali MA, Muhammad Low AL, Anouar EH, Youssef HM, Bahron H, et al. Palladium(II) complexes bearing N,O-bidentate Schiff base ligands: Experimental, in-silico, antibacterial, and catalytic properties. J Mol Struct. 2022;1260:132821.
20. Jovanović BŽ, Marinković AD, Assaleh FH, Csanádi J. Effect of substituents on the 13C chemical shifts of the azomethine carbon atom of N-(substituted phenylmethylene)-3- and -4-aminobenzoic acids. J Mol Struct. 2005;744-747:411-416.
21. Starke I, Koch A, Kammer S, Holdt HJ, Möller HM. Electrospray mass spectrometry and molecular modeling study of formation and stability of silver complexes with diazaperylene and bisisoquinoline. J Mass Spectrom. 2018;53(5):408-418.
22. Jović B, Negru N, Dimić D, Kordić B. Vibrational Spectroscopic and Quantum-Chemical Study of Indole–Ketone Hydrogen-Bonded Complexes. Molecules. 2025;30(13):2685.
23. Amani Jassim H, Sadiq AK, Nour Abd Alrazzak Abd A. Synthesis, Structural Characterization, and Anti-corrosion Study of a New Fluorinated Bis-Schiff Base. Applied Chemical Engineering. 2025.
24. Camellia FK, Ashrafuzzaman M, Islam MN, Banu LA, Zahan MK-E. Isoniazid Derived Schiff Base Metal Complexes: Synthesis, Characterization, Thermal Stability, Antibacterial and Antioxidant Activity Study. Asian Journal of Chemical Sciences. 2022:23-36.
25. Elsonbati A, Diab M, S. Y. Abbas SYA, Mohamed G, Morgan S. Preparation, Characterization and Biological Activity Screening on Some Metal Complexes Based of Schiff Base Ligand. Egyptian Journal of Chemistry. 2021;0(0):0-0.
26. Amer Saeed Jasim A, Tariq Hussein M. Synthesis , Characterization of New Poly Dentate Schiff Base ligand With Cu(II) ,Ag(I),Cd(II) ,and Pd(II) Complexes And Studying Their Biological Activity As Antioxidants And Anticancer. Journal of Kufa for Chemical Sciences. 2025;4(2):142-160.
27. Raman N, Joseph J, Velan ASK, Pothiraj C. Antifungal Activities of Biorelevant Complexes of Copper(II) with Biosensitive Macrocyclic Ligands. Mycobiology. 2006;34(4):214.
28. Sen SK, Barman UC, Manir MS, Mondal P, Dutta S, Paul M, et al. X-ray peak profile analysis of pure and Dy-doped α -MoO_3 nanobelts using Debye-Scherrer, Williamson-Hall and Halder-Wagner methods. Advances in Natural Sciences: Nanoscience and Nanotechnology. 2020;11(2):025004.
29. Moodi Z, Bagherzade G, Peters J. Quercetin as a Precursor for the Synthesis of Novel Nanoscale Cu (II) Complex as a Catalyst for Alcohol Oxidation with High Antibacterial Activity. Bioinorganic Chemistry and Applications. 2021;2021:1-9.
30. Table 6: Scavenging ability of DPPH free radical and ·OH free radical. PeerJ. http://dx.doi.org/10.7717/peerj.19357/table-6